A Massive Pulsar in a Compact Relativistic Binary

John Antoniadis,* Paulo C. C. Freire, Norbert Wex, Thomas M. Tauris, Ryan S. Lynch, Marten H. van Kerkwijk, Michael Kramer, Cees Bassa, Vik S. Dhillon, Thomas Driebe, Jason W. T. Hessels, Victoria M. Kaspi, Vladislav I. Kondratiev, Norbert Langer, Thomas R. Marsh, Maura A. McLaughlin, Timothy T. Pennucci, Scott M. Ransom, Ingrid H. Stairs, Joeri van Leeuwen, Joris P. W. Verbiest, David G. Whelan

Introduction: Neutron stars with masses above 1.8 solar masses ($M_\odot$), possess extreme gravitational fields, which may give rise to phenomena outside general relativity. Hitherto, these strong-field deviations have not been probed by experiment, because they become observable only in tight binaries containing a high-mass pulsar and where orbital decay resulting from emission of gravitational waves can be tested. Understanding the origin of such a system would also help to answer fundamental questions of close-binary evolution.

Methods: We report on radio-timing observations of the pulsar J0348+0432 and phase-resolved optical spectroscopy of its white-dwarf companion, which is in a 2.46-hour orbit. We used these to derive the component masses and orbital parameters, infer the system's motion, and constrain its age.

Results: We find that the white dwarf has a mass of 0.172 ± 0.003 $M_\odot$, which, combined with orbital velocity measurements, yields a pulsar mass of 2.01 ± 0.04 $M_\odot$. Additionally, over a span of 2 years, we observed a significant decrease in the orbital period, $\dot{P}_b^{obs} = -8.6 \pm 1.4$ μs year^{-1} in our radio-timing data.

Discussion: Pulsar J0348+0432 is only the second neutron star with a precisely determined mass of 2 $M_\odot$ and independently confirms the existence of such massive neutron stars in nature. For these masses and orbital period, general relativity predicts a significant orbital decay, which matches the observed value, $\dot{P}_b^{obs}/\dot{P}_b^{GR} = 1.05 \pm 0.18$.

The pulsar has a gravitational binding energy 60% higher than other known neutron stars in binaries where gravitational-wave damping has been detected. Because the magnitude of strong-field deviations generally depends nonlinearly on the binding energy, the measurement of orbital decay transforms the system into a gravitational laboratory for an as-yet untested gravity regime. The consistency of the observed orbital decay with general relativity therefore supports its validity, even for such extreme gravity-matter couplings, and rules out strong-field phenomena predicted by physically well-motivated alternatives. Moreover, our result supports the use of general relativity–based templates for the detection of gravitational waves from merger events with advanced ground-based detectors.

Lastly, the system provides insight into pulsar-spin evolution after mass accretion. Because of its short merging time scale of 400 megayears, the system is a direct channel for the formation of an ultracompact x-ray binary, possibly leading to a pulsar-planet system or the formation of a black hole.

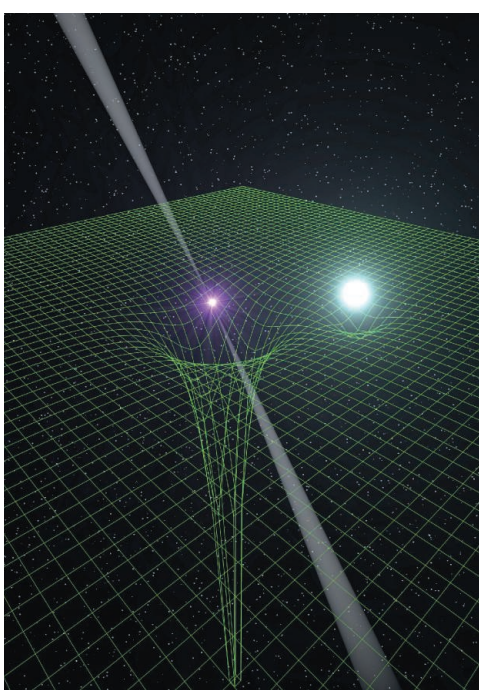

Artist's impression of the PSR J0348+0432 system. The compact pulsar (with beams of radio emission) produces a strong distortion of spacetime (illustrated by the green mesh). Conversely, spacetime around its white dwarf companion (in light blue) is substantially less curved. According to relativistic theories of gravity, the binary system is subject to energy loss by gravitational waves.

The list of author affiliations is available in the full article online.
*Corresponding author. E-mail: jantoniadis@mpifr-bonn.mpg.de

READ THE FULL ARTICLE ONLINE
http://dx.doi.org/10.1126/science.1233232

Cite this article as J. Antoniadis *et al.*, *Science* **340**, 1233232 (2013). DOI: 10.1126/science.1233232

FIGURES AND TABLE IN THE FULL ARTICLE

SUPPLEMENTARY MATERIALS

Supplementary Text
Figs. S1 to S11
Tables S1 to S3
References

ADDITIONAL RESOURCES

Fundamental Physics in Radio Astronomy group at the Max-Planck-Institut für Radioastronomie, www3.mpifr-bonn.mpg.de/div/fundamental/

The European Southern Observatory, www.eso.org/public/

D. R. Lorimer, Binary and millisecond pulsars. *Living Rev. Relativ.* **11**, 8 (2008). http://dx.doi.org/10.12942/lrr-2008-8

T. Damour, "Binary systems as test-beds of gravity theories," in *Physics of Relativistic Objects in Compact Binaries: From Birth to Coalescence*, M. Colpi, P. Casella, V. Gorini, U. Moschella, A. Possenti, Eds. (Astrophysics and Space Science Library, Springer, Dordrecht, Netherlands, 2009), vol. 359, pp. 1–41.

A Massive Pulsar in a Compact Relativistic Binary

John Antoniadis,[1]* Paulo C. C. Freire,[1] Norbert Wex,[1] Thomas M. Tauris,[2,1] Ryan S. Lynch,[3] Marten H. van Kerkwijk,[4] Michael Kramer,[1,5] Cees Bassa,[5] Vik S. Dhillon,[6] Thomas Driebe,[7] Jason W. T. Hessels,[8,9] Victoria M. Kaspi,[3] Vladislav I. Kondratiev,[8,10] Norbert Langer,[2] Thomas R. Marsh,[11] Maura A. McLaughlin,[12] Timothy T. Pennucci,[13] Scott M. Ransom,[14] Ingrid H. Stairs,[15] Joeri van Leeuwen,[8,9] Joris P. W. Verbiest,[1] David G. Whelan[13]

Many physically motivated extensions to general relativity (GR) predict substantial deviations in the properties of spacetime surrounding massive neutron stars. We report the measurement of a 2.01 ± 0.04 solar mass ($M_\odot$) pulsar in a 2.46-hour orbit with a 0.172 ± 0.003 $M_\odot$ white dwarf. The high pulsar mass and the compact orbit make this system a sensitive laboratory of a previously untested strong-field gravity regime. Thus far, the observed orbital decay agrees with GR, supporting its validity even for the extreme conditions present in the system. The resulting constraints on deviations support the use of GR-based templates for ground-based gravitational wave detectors. Additionally, the system strengthens recent constraints on the properties of dense matter and provides insight to binary stellar astrophysics and pulsar recycling.

Neutron stars (NSs) with masses above 1.8 solar mass ($M_\odot$) manifested as radio pulsars are valuable probes of fundamental physics in extreme conditions unique in the observable universe and inaccessible to terrestrial experiments. Their high masses are directly linked to the equation-of-state (EOS) of matter at supranuclear densities (*1*, *2*) and constrain the lower mass limit for production of astrophysical black holes (BHs). Furthermore, they possess extreme internal gravitational fields, which result in gravitational binding energies substantially higher than those found in more common, 1.4-$M_\odot$ NSs. Modifications to general relativity (GR), often motivated by the desire for a unified model of the four fundamental forces, can generally imprint measurable signatures in the gravitational waves (GWs) radiated by systems containing such objects, even if deviations from GR vanish in the solar system and in less-massive NSs (*3*–*5*).

However, the most massive NSs known today reside in long-period binaries or other systems unsuitable for GW radiation tests. Identifying a massive NS in a compact, relativistic binary is thus of key importance for understanding gravity-matter coupling under extreme conditions. Furthermore, the existence of a massive NS in a relativistic orbit can also be used to test current knowledge of close binary evolution.

Results

PSR J0348+0432 and Optical Observations of Its Companion

PSR J0348+0432, a pulsar spinning at 39 ms in a 2.46-hour orbit with a low-mass companion, was detected by a recent survey (*6*, *7*) conducted with the Robert C. Byrd Green Bank Telescope (GBT). Initial timing observations of the binary yielded an accurate astrometric position, which allowed us to identify its optical counterpart in the Sloan Digital Sky Survey (SDSS) archive (*8*). The colors and flux of the counterpart are consistent with a low-mass white dwarf (WD) with a helium core at a distance of $d \sim 2.1$ kpc. Its relatively high apparent brightness ($g' = 20.71 \pm 0.03$ mag) allowed us to resolve its spectrum by using the Apache Point Optical Telescope. These observations revealed deep hydrogen lines, typical of low-mass WDs, confirming our preliminary identification. The radial velocities of the WD mirrored that of PSR J0348+0432, also verifying that the two stars are gravitationally bound.

In December 2011, we obtained phase-resolved spectra of the optical counterpart by using the FORS2 spectrograph of the Very Large Telescope (VLT). For each spectrum, we measured the radial velocity, which we then folded modulo the system's orbital period. Our orbital fit to the velocities constrains the semiamplitude of their modulation to be $K_{WD} = 351 \pm 4$ km s^{-1} (1-σ confidence interval) (Fig. 1; see also Materials and Methods). Similarly, the orbital solution from radio-pulsar timing yields $K_{PSR} = 30.008235 \pm 0.000016$ km s^{-1} for the pulsar. Combined, these constraints imply a mass ratio, $q = M_{PSR}/M_{WD} = K_{WD}/K_{PSR} = 11.70 \pm 0.13$.

Modeling of the Balmer-series lines in a high signal-to-noise average spectrum formed by the coherent addition of individual spectra (Fig. 1B) shows that the WD has an effective temperature of $T_{eff} = 10{,}120 \pm 47_{stat} \pm 90_{sys}$ K and a surface gravity of $\log_{10}[g\ (\mathrm{cm\ s^{-2}})] = 6.035 \pm 0.032_{stat} \pm 0.060_{sys}$ dex. Here, the systematic error is an overall estimate of uncertainties resulting from our fitting technique and flux calibration (*8*). We found no correlation of this measurement with orbital phase and no signs of rotationally induced broadening in the spectral lines (*8*). Furthermore, we searched for variability by using the ULTRACAM instrument (*9*) on the 4.2-m William-Herschel Telescope in La Palma, Spain. The light curves (fig. S3), spanning 3 hours in total, have a root-mean-square (rms) scatter of ~0.53, 0.07, and 0.08 mag in u', g', and r', respectively, and show no evidence for variability over the course of the observations. The phase-folded light curve shows no variability either. Additionally, our calibrated magnitudes are consistent with the SDSS catalog magnitudes, implying that the WD shone at a constant flux over this ~5 year time scale (*8*).

Mass of the White Dwarf

The surface gravity of the WD scales with its mass and the inverse square of its radius ($g \equiv GM_{WD}/R_{WD}^2$, where G is Newton's gravitational constant). Thus, the observational constraints combined with a theoretical finite-temperature mass-radius relation for low-mass WDs yield a unique solution for the mass of the companion (*10*). Numerous such models exist in the literature, the most detailed of which are in good agreement for very-low-mass WDs (<0.17 to 0.18 $M_\odot$) but differ substantially for higher masses [e.g., (*11*–*13*)]. The main reason for this is the difference in the predicted size of the hydrogen envelope, which determines whether the main energy source of the star is residual hydrogen burning (for "thick" envelopes) or the latent heat of the core (for "thin" envelopes).

In the most widely accepted scenario, WDs lose their thick hydrogen envelope only if their mass exceeds a threshold. The exact location of the latter is still uncertain but estimated to be around 0.17 to 0.22 $M_\odot$ [e.g., (*11*–*13*)]. Two other pulsars with WD companions, studied in the literature, strongly suggest that this transition threshold is indeed most likely close to 0.2 $M_\odot$ (*10*, *14*). In particular, PSR J1909−3744 has a large characteristic age of several gigayears (Gy) and a WD

[1]Max-Planck-Institut für Radioastronomie, Auf dem Hügel 69, 53121 Bonn, Germany. [2]Argelander Institut für Astronomie, Auf dem Hügel 71, 53121 Bonn, Germany. [3]Department of Physics, McGill University, 3600 University Street, Montreal, QC H3A 2T8, Canada. [4]Department of Astronomy and Astrophysics, University of Toronto, 50 St. George Street, Toronto, ON M5S 3H4, Canada. [5]Jodrell Bank Centre for Astrophysics, The University of Manchester, Alan Turing Building, Manchester M13 9PL, UK. [6]Department of Physics and Astronomy, University of Sheffield, Sheffield S3 7RH, UK. [7]Deutsches Zentrum für Luft- und Raumfahrt e.V. (DLR), Raumfahrtmanagement, Königswinterer Str. 522-524, 53227 Bonn, Germany. [8]ASTRON, the Netherlands Institute for Radio Astronomy, Postbus 2, 7990 AA Dwingeloo, Netherlands. [9]Astronomical Institute Anton Pannekoek, University of Amsterdam, Science Park 904, 1098 XH Amsterdam, Netherlands. [10]Astro Space Center of the Lebedev Physical Institute, Profsoyuznaya str. 84/32, Moscow 117997, Russia. [11]Department of Physics, University of Warwick, Coventry CV4 7AL, UK. [12]Department of Physics, West Virginia University, 111 White Hall, Morgantown, WV 26506, USA. [13]Department of Astronomy, University of Virginia, Post Office Box 400325, Charlottesville, VA 22904, USA. [14]National Radio Astronomy Observatory, 520 Edgemont Road, Charlottesville, VA 22903, USA. [15]Department of Physics and Astronomy, University of British Columbia, 6224 Agricultural Road, Vancouver, BC V6T 1Z1, Canada.

*Corresponding author. E-mail: jantoniadis@mpifr-bonn.mpg.de

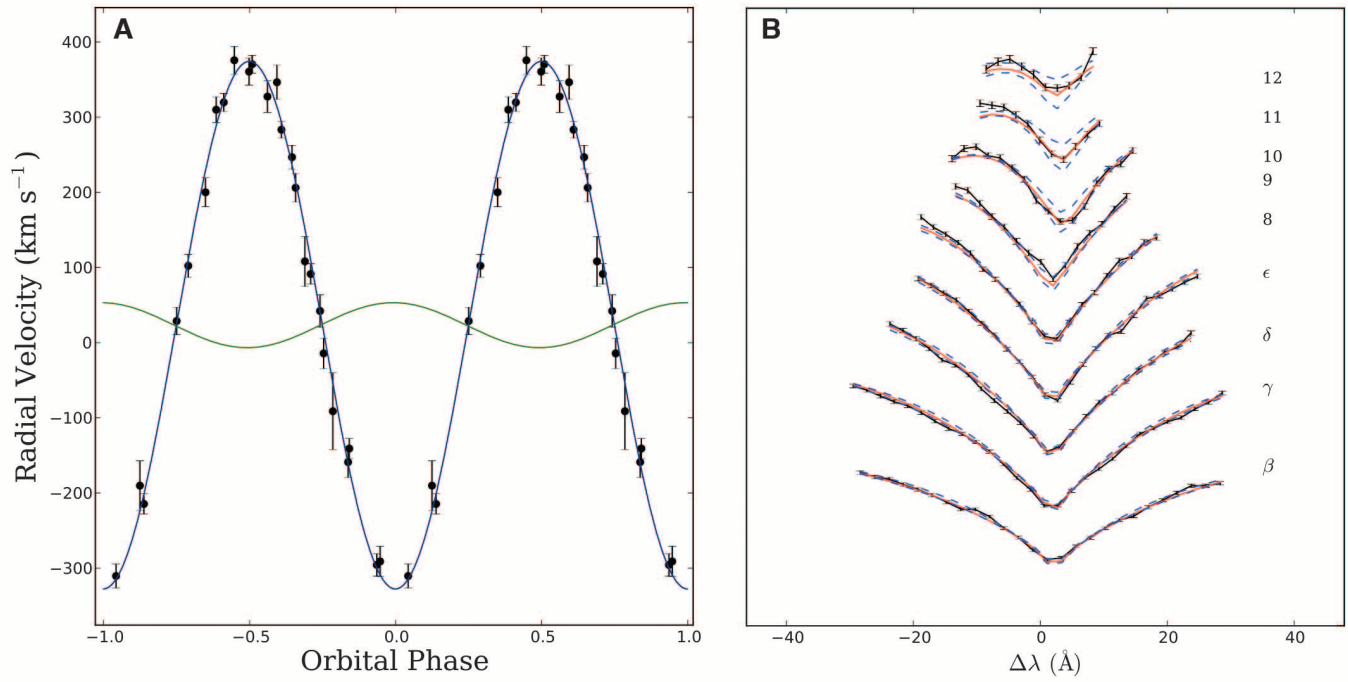

Fig. 1. Radial velocities and spectrum of the white dwarf companion to PSR J0348+0432. (**A**) Radial velocities of the WD companion to PSR J0348+0432 plotted against the orbital phase (shown twice for clarity). Overplotted is the best-fit orbit of the WD (blue line) and the mirror orbit of the pulsar (green). Error bars indicate 1-σ confidence intervals. (**B**) Details of the fit to the Balmer lines (Hβ to H12) in the average spectrum of the WD companion to PSR J0348+0432 created by the coherent addition of 26 individual spectra shifted to zero velocity. Lines from Hβ (bottom) to H12 are shown. The red solid lines are the best-fit atmospheric model (see text). Two models, one with $T_{\rm eff}$ = 9900 K and $\log_{10}g$ = 5.70 and one with $T_{\rm eff}$ = 10,200 K and $\log_{10}g$ = 6.30, each ~ 3-σ off from the best-fit central value (including systematics), are shown for comparison (dashed blue lines).

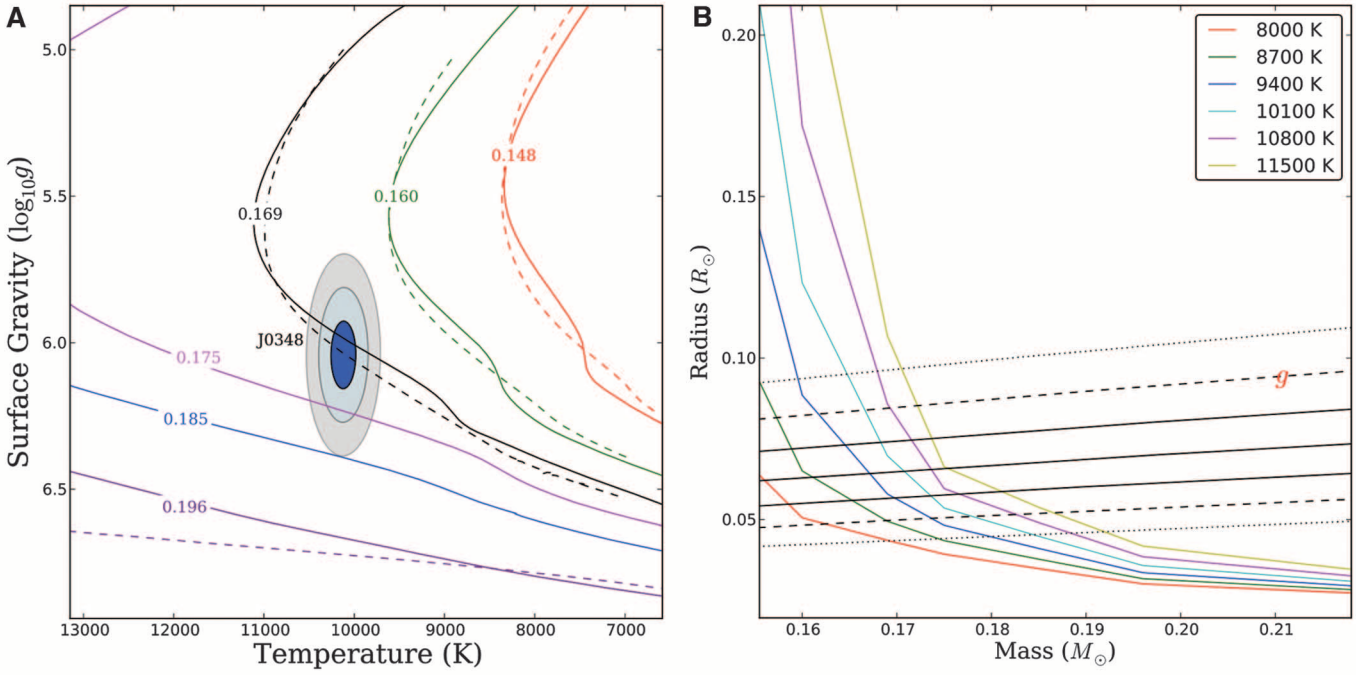

Fig. 2. Mass measurement of the white dwarf companion to PSR J0348+0432. (**A**) Constraints on $T_{\rm eff}$ and g for the WD companion to PSR J0348+0432 compared with theoretical WD models. The shaded areas depict the $\chi^2 - \chi^2_{\rm min}$ = 2.3, 6.2, and 11.8 intervals (equivalent to 1-, 2-, and 3-σ) of our fit to the average spectrum. Dashed lines show the detailed theoretical cooling models of (*11*). Continuous lines depict tracks with thick envelopes for masses up to ~0.2 $M_\odot$ that yield the most conservative constraints for the mass of the WD. (**B**) Finite-temperature mass-radius relations for our models together with the constraints imposed from modeling of the spectrum. Low mass–high temperature points are an extrapolation from lower temperatures.

companion with a well-determined mass of 0.20 $M_\odot$ (*15*) that appears to be hot (*10*), suggesting that its envelope is thick. For this reason, we base the WD mass estimate on cooling tracks with thick hydrogen atmospheres for masses up to 0.2 $M_\odot$, which we constructed by using the MESA stellar evolution code (*8*, *16*). Initial models were built for masses identical to the ones in (*11*), for which previous comparisons have yielded good agreement with observations (*14*), with the addition of tracks with 0.175 and 0.185 $M_\odot$ for finer coverage (Fig. 2). For masses up to 0.169 $M_\odot$, our models show excellent agreement with (*11*); however, our 0.196 $M_\odot$ model is quite different, because it has a thick envelope instead of a thin one. Being closer to the constraints for the WD companion to PSR J0348+0432, it yields a more conservative mass constraint, M_{WD} = 0.165 to 0.185 at 99.73% confidence (Fig. 3 and Table 1), which we adopt. The corresponding radius is R_{WD} = 0.046 to 0.092 $R_\odot$ at 99.73% confidence. Our models yield a cooling age of $\tau_{cool} \sim 2$ Gy.

Pulsar Mass

The derived WD mass and the observed mass ratio q imply a NS mass in the range from 1.97 to 2.05 $M_\odot$ at 68.27% or 1.90 to 2.18 $M_\odot$ at 99.73% confidence. Hence, PSR J0348+0432 is only the second NS with a precisely determined mass around 2 $M_\odot$, after PSR J1614−2230 (*2*). It has a 3-σ lower mass limit 0.05 $M_\odot$ higher than the latter and therefore provides a verification, using a different method, of the constraints on the EOS of superdense matter present in NS interiors (*2*, *17*). For these masses and the known orbital period, GR predicts that the orbital period should decrease at the rate of $\dot{P}_b^{GR} = (-2.58^{+0.07}_{-0.11}) \times 10^{-13}$ s s^{-1} (68.27% confidence) because of energy loss through GW emission.

Radio Observations

Since April 2011, we have been observing PSR J0348+0432 with the 1.4-GHz receiver of the 305-m radio telescope at the Arecibo Observatory by using its four wide-band pulsar processors (*18*). In order to verify the Arecibo data, we have been independently timing PSR J0348+0432 at 1.4 GHz by using the 100-m radio telescope in Effelsberg, Germany. The two timing data sets produce consistent rotational models, providing added confidence in both. Combining the Arecibo and Effelsberg data with the initial GBT observations (*7*), we derived the timing solution presented in Table 1. To match the arrival times, the solution requires a significant measurement of orbital decay, $\dot{P}_b = -2.73 \times 10^{-13} \pm 0.45 \times 10^{-13}$ s s^{-1} (68.27% confidence).

The total proper motion and distance estimate (Table 1) allowed us to calculate the kinematic corrections to $\dot{P}_b$ from its motion in the Galaxy, plus any contribution from possible variations of G: $\delta\dot{P}_b = 0.016 \times 10^{-13} \pm 0.003 \times 10^{-13}$ s s^{-1}. This is negligible compared to the measurement uncertainty. Similarly, the small rate of rotational energy loss of the pulsar (Table 1) excludes any substantial contamination resulting from mass loss from the system; furthermore, we can exclude substantial contributions to $\dot{P}_b$ from tidal effects [see (*8*) for details]. Therefore, the observed $\dot{P}_b$ is caused by GW emission, and its magnitude is entirely consistent with the one predicted by GR: $\dot{P}_b/\dot{P}_b^{GR} = 1.05 \pm 0.18$ (Fig. 3).

If we assume that GR is the correct theory of gravity, we can then derive the component masses from the intersection of the regions allowed by q and $\dot{P}_b$ (Fig. 3): $M_{WD} = 0.177^{+0.017}_{-0.018}$ $M_\odot$ and $M_{PSR} = 2.07^{+0.20}_{-0.21}$ $M_\odot$ (68.27% confidence). These values are not too constraining yet. However, the uncertainty of the measurement of $\dot{P}_b$ decreases with $T_{baseline}^{-5/2}$ (where $T_{baseline}$ is the timing baseline); therefore, this method will yield very precise mass measurements within a couple of years.

Discussion

PSR J0348+0432 as a Testbed for Gravity

There are strong arguments for GR not to be valid beyond a (yet unknown) critical point, like its incompatibility with quantum theory and its prediction of the formation of spacetime singularities. Therefore, it remains an open question whether GR is the final description of macroscopic gravity. This strongly motivates testing gravity regimes that have not been tested before, in particular regimes where gravity is strong and highly nonlinear. Presently, binary pulsars provide the best high-precision experiments to probe strong-field deviations from GR and the best tests of the radiative properties of gravity (*19*–*23*). The orbital period of PSR J0348+0432 is only 15 s longer than that of the double pulsar system PSR J0737–3039, but it has ~two times more fractional gravitational binding energy than each of the double-pulsar NSs. This places it far outside the presently tested binding energy range (Fig. 4A) (*8*). Because the magnitude of strong-field effects generally depends nonlinearly on the binding energy, the measurement of orbital decay transforms the

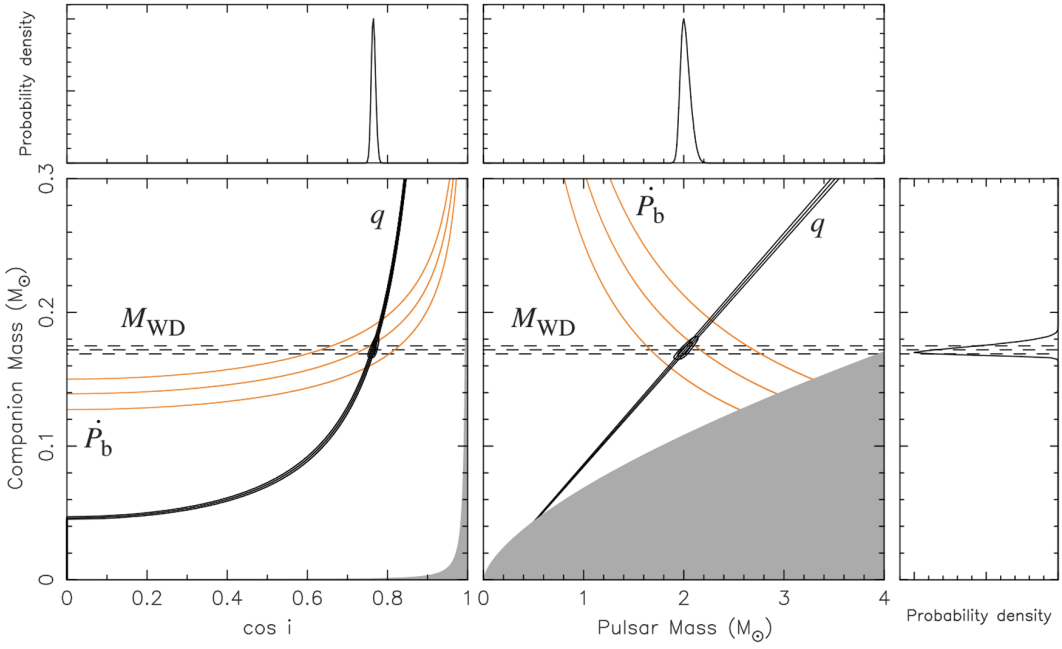

Fig. 3. System masses and orbital-inclination constraints. Constraints on system masses and orbital inclination from radio and optical measurements of PSR J0348+0432 and its WD companion. Each triplet of curves corresponds to the most likely value and standard deviations (68.27% confidence) of the respective parameters. Of these, two (q and M_{WD}) are independent of specific gravity theories (in black). The contours contain the 68.27 and 95.45% of the two-dimensional probability distribution. The constraints from the measured intrinsic orbital decay ($\dot{P}_b^{int}$, in orange) are calculated assuming that GR is the correct theory of gravity. All curves intersect in the same region, meaning that GR passes this radiative test (*8*). (**Bottom left**) cos$i$-M_{WD} plane. The gray region is excluded by the condition $M_{PSR} > 0$. (**Bottom right**) M_{PSR}-M_{WD} plane. The gray region is excluded by the condition sin$i \leq 1$. The lateral graphs depict the one-dimensional probability-distribution function for the WD mass (**right**), pulsar mass (**top right**), and inclination (**top left**) based on the mass function, M_{WD}, and q.

system into a gravitational laboratory for a previously untested regime, qualitatively very different from what was accessible in the past.

In physically consistent and extensively studied alternatives, gravity is generally mediated by extra fields (e.g., scalar) in addition to the tensor field of GR (*5*). A dynamical coupling between matter and these extra fields can lead to prominent deviations from GR that only occur at the high gravitational binding energies of massive NSs. One of the prime examples is the strong-field scalarization discovered in (*3*). If GR is not valid, in the PSR J0348+0432 system where such an object is closely orbited by a weakly self-gravitating body, one generally expects a violation of the strong equivalence principle that in turn leads to a modification in the emission of GWs. Although in GR the lowest source multipole that generates gravitational radiation is the quadrupole, alternative gravity theories generally predict the presence of monopole and dipole radiation on top of a modification of the other multipoles (*5*). For a binary system, the leading change in the orbital period is then given by the dipole contribution, which for a (nearly) circular orbit reads (*8*)

$$\dot{P}_{\rm b}^{\rm dipolar} \simeq -\frac{4\pi^2 G}{c^3 P_{\rm b}} \frac{M_{\rm PSR} M_{\rm WD}}{M_{\rm PSR}+M_{\rm WD}} (\alpha_{\rm PSR}-\alpha_{\rm WD})^2 \quad (1)$$

where $\alpha_{\rm PSR}$ is the effective coupling strength between the NS and the ambient fields responsible for the dipole moment (e.g., scalar fields in scalar-tensor gravity) and $\alpha_{\rm WD}$ is the same parameter for the WD companion. The WD companion to PSR J0348+0432 has a fractional gravitational binding energy ($E_{\rm grav}/M_{\rm WD}c^2$) of just -1.2×10^{-5} and is therefore a weakly self-gravitating object. Consequently, $\alpha_{\rm WD}$ is practically identical to the linear field-matter coupling α_0, which is well constrained ($|\alpha_0| < 0.004$) in solar system experiments (*20*, *24*).

For $\alpha_{\rm PSR}$, the situation is very different. Even if α_0 is vanishingly small, $\alpha_{\rm PSR}$ can have values close to unity, because of a nonlinear behavior of gravity in the interaction between matter and the gravitational fields in the strong-gravity regime inside NSs (*3*, *4*). A significant $\alpha_{\rm PSR}$ for NSs up to 1.47 $M_\odot$ has been excluded by various binary pulsar experiments (*8*, *23*). The consistency of the observed GW damping ($\dot{P}_{\rm b}$) with the GR predictions for PSR J0348+0432 (Table 1) implies $|\alpha_{\rm PSR}-\alpha_0| < 0.005$ (95% confidence) and consequently excludes significant strong-field deviations, even for massive NSs of ~2 $M_\odot$.

To demonstrate in some detail the implications of our results for possible strong-field deviations of gravity from Einstein's theory, we confront our limits on dipolar radiation with a specific class of scalar-tensor theories, in which gravity is mediated by a symmetric second-rank tensor field, $g_{\mu\nu}$*, and by a long-range (massless) scalar field, φ. Scalar-tensor theories are well motivated and consistent theories of gravity, extensively studied in the literature [e.g., (*25*, *26*)]. For this reason, they are the most natural framework for us to illustrate the gravitational phenomena that can be probed with PSR J0348+0432.

Concerning the EOS of NS matter, in our calculations we use the rather stiff EOS ".20" of (*27*) that supports (in GR) NSs of up to 2.6 $M_\odot$. We make this choice for two reasons: (i) A stiffer EOS generally leads to more conservative limits when constraining alternative gravity theories, and (ii) it is able to support even more massive NSs than PSR J0348+0432, which are likely to exist (*28*–*30*). Furthermore, in most of our conclusions a specific EOS is used only for illustrative purposes, and the obtained generic results are EOS independent.

Figure 4B illustrates how PSR J0348+0432 probes a nonlinear regime of gravity that has not been tested before. A change in EOS and gravity theory would lead to a modified functional shape for $\alpha_{\rm PSR}$. However, this would not change the general picture: Even in the strong gravitational

Table 1. Observed and derived parameters for the PSR J0348+0432 system. Timing parameters for the PSR J0348+0432 system, indicated with their 1-σ uncertainties as derived by tempo2 where appropriate (numbers in parentheses refer to errors on the last digits). The timing parameters are calculated for the reference epoch modified Julian date (MJD) 56000 and are derived from TOAs in the range MJD 54872 to 56208.

Optical parameters	
Effective temperature, $T_{\rm eff}$ (K)	$10120 \pm 47_{\rm stat} \pm 90_{\rm sys}$
Surface gravity, $\log_{10}[g(\mathrm{cm\ s^{-1}})]$	$6.035 \pm 0.032_{\rm stat} \pm 0.060_{\rm sys}$
Semiamplitude of orbital radial velocity, $K_{\rm WD}$ (km $\mathrm{s^{-1}}$)	351 ± 4
Systemic radial velocity relative to the Sun, γ (km $\mathrm{s^{-1}}$)	-1 ± 20
Timing parameters	
Right ascension, α (J2000)	$03^{\rm h}\ 48^{\rm m}\ 43^{\rm s}.639000(4)$
Declination, δ (J2000)	$+04°\ 32'\ 11.''4580(2)$
Proper motion in right ascension, μ_α (mas $\mathrm{year^{-1}}$)	+4.04(16)
Proper motion in declination, μ_δ (mas $\mathrm{year^{-1}}$)	+3.5(6)
Parallax, $\pi_{\rm d}$ (mas)	0.47*
Spin frequency, ν (Hz)	25.5606361937675(4)
First derivative of ν, $\dot{\nu}$ (10^{-15} Hz $\mathrm{s^{-1}}$)	−0.15729(3)
Dispersion measure, DM ($\mathrm{cm^{-3}}$ pc)	40.46313(11)
First derivative of DM, DM1 ($\mathrm{cm^{-3}}$ pc $\mathrm{year^{-1}}$)	−0.00069(14)
Orbital period, $P_{\rm b}$ (day)	0.102424062722(7)
Time of ascending node, $T_{\rm asc}$ (MJD)	56000.084771047(11)
Projected semimajor axis of the pulsar orbit, x (lt-s)	0.14097938(7)
$\eta \equiv e\sin\omega$	$+1.9 \times 10^{-6} \pm 1.0 \times 10^{-6}$
$\kappa \equiv e\cos\omega$	$+1.4 \times 10^{-6} \pm 1.0 \times 10^{-6}$
First derivative of $P_{\rm b}$, $\dot{P}_{\rm b}$ (10^{-12} s $\mathrm{s^{-1}}$)	−0.273(45)
Derived parameters	
Galactic longitude, l	183.°3368
Galactic latitude, b	−36.°7736
Distance, d (kpc)	2.1(2)
Total proper motion, μ (mas $\mathrm{year^{-1}}$)	5.3(4)
Spin period, P (ms)	39.1226569017806(5)
First derivative of P, $\dot{P}$ (10^{-18} s $\mathrm{s^{-1}}$)	0.24073(4)
Characteristic age, $\tau_{\rm c}$ (Gy)	2.6
Transverse magnetic field at the poles, B_0 (10^9 G)	~2
Rate or rotational energy loss, $\dot{E}$ (10^{32} erg $\mathrm{s^{-1}}$)	~1.6
Mass function, f ($M_\odot$)	0.000286778(4)
Mass ratio, $q \equiv M_{\rm PSR}/M_{\rm WD}$	11.70(13)
White dwarf mass, $M_{\rm WD}$ ($M_\odot$)	0.172(3)
Pulsar mass, $M_{\rm PSR}$ ($M_\odot$)	2.01(4)
"Range" parameter of Shapiro delay, r (μs)	0.84718*
"Shape" parameter of Shapiro delay, $s \equiv \sin i$	0.64546*
White dwarf radius, $R_{\rm WD}$ ($R_\odot$)	0.065(5)
Orbital separation, a (10^9 m)	0.832
Orbital separation, a ($R_\odot$)	1.20
Orbital inclination, i	40.°2(6)
$\dot{P}_{\rm b}$ predicted by GR, $\dot{P}_{\rm b}^{\rm GR}$ (10^{-12} s $\mathrm{s^{-1}}$)	$-0.258^{+0.008}_{-0.011}$
$\dot{P}_{\rm b}/\dot{P}_{\rm b}^{\rm GR}$	1.05 ± 0.18
Time until coalescence, $\tau_{\rm m}$ (My)	~400

*For these timing parameters, we adopted the optically derived parameters (see text for details).

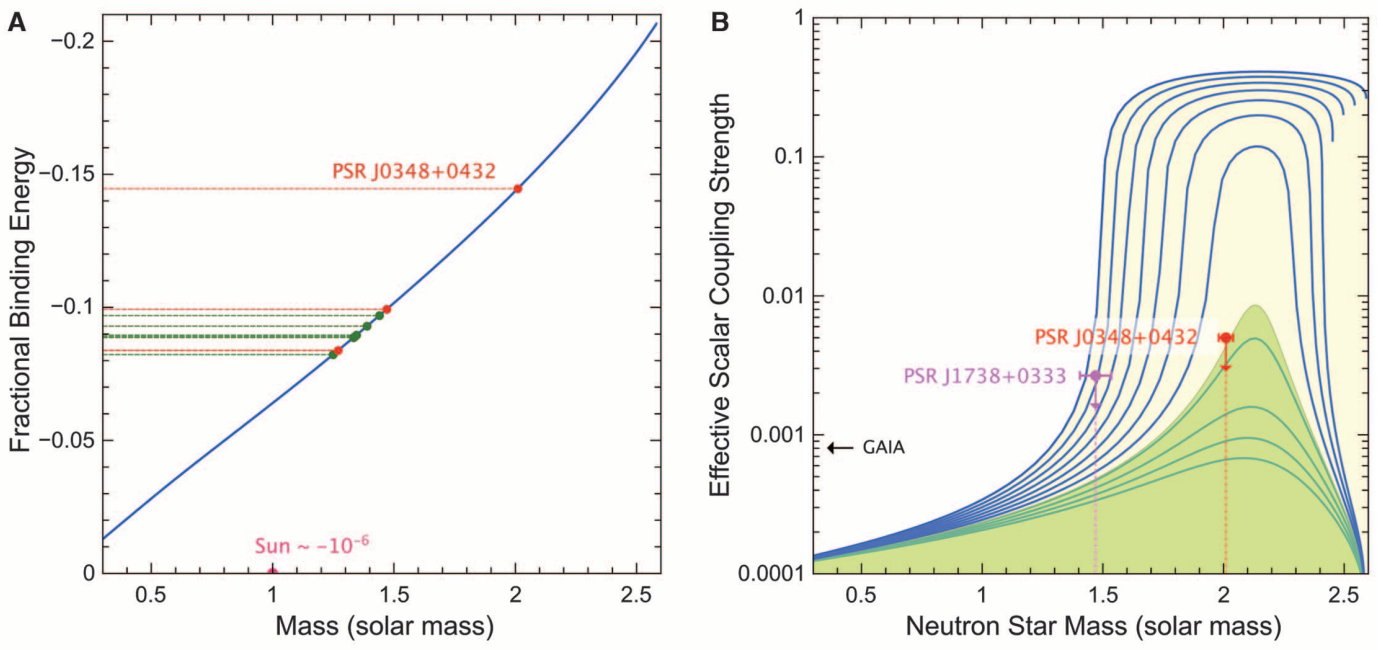

Fig. 4. Probing strong field gravity with PSR J0348+0432. (**A**) Fractional gravitational binding energy as a function of the inertial mass of a NS in GR (blue curve). The dots indicate the NSs of relativistic NS-NS (in green) and NS-WD (in red) binary-pulsar systems currently used for precision gravity tests (*8*). (**B**) Effective scalar coupling as a function of the NS mass, in the "quadratic" scalar-tensor theory of (*4*). For the linear coupling of matter to the scalar field, we have chosen $\alpha_0 = 10^{-4}$, a value well below the sensitivity of any near-future solar system experiment [e.g., GAIA (*62*)]. The solid curves correspond to stable NS configurations for different values of the quadratic coupling β_0: −5 to −4 (top to bottom) in steps of 0.1. The yellow area indicates the parameter space allowed by the best current limit on $|\alpha_{PSR} - \alpha_0|$ (*23*), whereas only the green area is in agreement with the limit presented here.

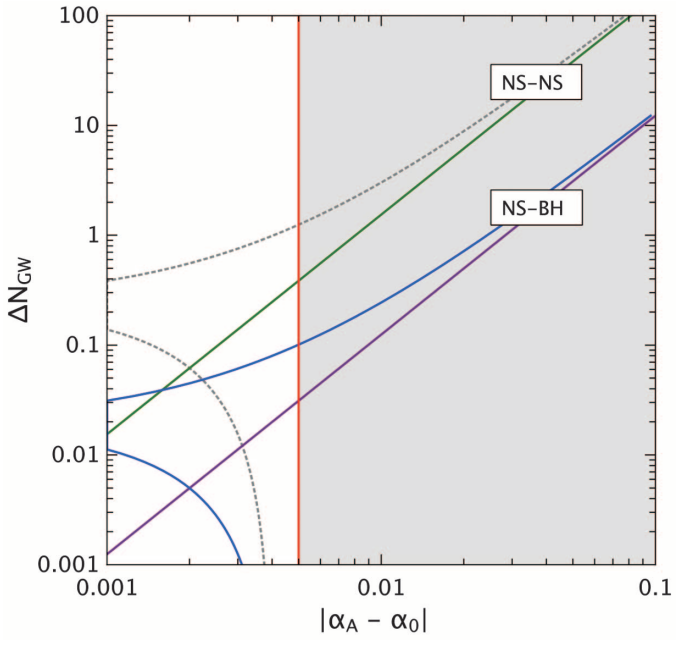

Fig. 5. Constraints on the phase offset in gravitational wave cycles in the LIGO/VIRGO bands. Maximum offset in GW cycles in the LIGO/VIRGO band (20 Hz to a few kHz) between the GR template and the true phase evolution of the in-spiral in the presence of dipolar radiation as a function of the effective coupling of the massive NS for two different system configurations: a 2 $M_\odot$ NS with a 1.25 $M_\odot$ NS (NS-NS) and a merger of a 2 $M_\odot$ NS with a 10 $M_\odot$ BH (NS-BH). In the NS-NS case, the green line is for $\alpha_B = \alpha_0$, and the gray dotted line represents the most conservative, rather unphysical, assumption $\alpha_0 = 0.004$ and $\alpha_B = 0$ (*8*). In the NS-BH case, α_B is set to zero (from the assumption that no-hair theorems hold). The blue line is for $\alpha_0 = 0.004$ (solar system limit for scalar-tensor theories), and the purple line represents $\alpha_0 = 0$. The gray area to the right of the red line is excluded by PSR J0348+0432. In this plot, there is no assumption concerning the EOS.

field of a 2 $M_\odot$ NS, gravity seems to be well described by GR, and there is little space for any deviations, at least in the form of long-range fields, which influence the binary dynamics. Short-range interactions, like massive Brans-Dicke gravity (*31*) with a sufficiently large scalar mass (heavier than ~10^{-19} eV/c^2), cannot be excluded by PSR J0348+0432.

Constraints on the Phase Evolution of Neutron Star Mergers

One of the most promising sources of GWs that might be detected by ground-based laser interferometers like the LIGO [Laser Interferometer Gravitational Wave Observatory (*32*)] and the VIRGO (*33*) projects (*34*) are in-spiraling compact binaries, consisting of NSs and BHs, whose orbits are decaying toward a final coalescence because of GW damping. As the signal sweeps in frequency through the detectors' typical sensitive bandwidth between about 20 Hz and a few kHz, the GW signal will be deeply buried in the broadband noise of the detectors (*34*). To detect it, one will have to apply a matched filtering technique, that is, correlate the output of the detector with a template wave form. Consequently, it is crucial to know the binary's orbital phase with high accuracy for searching and analyzing the signals from in-spiraling compact binaries. Typically, one aims to lose less than one GW cycle in a signal with ~10^4 cycles. For this reason, within GR such calculations have been conducted with great effort by various groups up to the 3.5 post-Newtonian order, that is, all (nonvanishing) terms up to order $(v/c)^7$ (where v is relative orbital velocity of the binary's components), providing sufficient accuracy for a detection (*35*–*37*).

If the gravitational interaction between two compact masses is different from GR, the phase evolution over the last few thousand cycles, which fall into the bandwidth of the detectors, might be too different from the (GR) template to extract

the signal from the noise. In scalar-tensor gravity, for instance, the evolution of the phase is driven by radiation reaction, which is modified because the system loses energy to scalar GWs (*38*, *39*). Depending on the difference between the effective scalar couplings of the two bodies, α_A and α_B, the 1.5 post-Newtonian dipolar contribution to the phase evolution could drive the GW signal many cycles away from the GR template. For this reason, it is desirable that potential deviations from GR in the interaction of two compact objects can be tested and constrained before the start of the advanced GW detectors. For "canonical" 1.4 $M_\odot$ NSs and long-range gravitational fields, this has already been achieved to a high degree in binary pulsar experiments, for example, (*39*). So far, the best constraints on dipolar gravitational wave damping in compact binaries come from the observations of the millisecond pulsar PSR J1738+0333 (*23*). However, as discussed in detail above, these timing experiments are insensitive to strong-field deviations that might only become relevant in the strong gravitational fields associated with high-mass NSs. Consequently, the dynamics of a merger of a 2 $M_\odot$ NS with a "canonical" NS or a BH might have a significant contribution from dipolar GWs. With our constraints on dipolar radiation damping from the timing observations of PSR J0348+0432, given above, we can already exclude a deviation of more than ~0.5 cycles from the GR template during the observable in-spiral caused by additional long-range gravitational fields for the whole range of NS masses observed in nature [see Fig. 5 and (*8*) for the details of the calculation]. This compares to the precision of GR templates based on the 3.5 post-Newtonian approximation (*35*, *37*). Furthermore, in an extension of the arguments in (*38*, *39*) to massive NSs, our result implies that binary pulsar experiments are already more sensitive for testing such deviations than the upcoming advanced GW detectors.

Lastly, as mentioned before, our results on PSR J0348+0432 cannot exclude dipolar radiation from short-range fields. Hence, if the range of the additional field in the gravitational interaction happens to lie between the wavelength of the GWs of PSR J0348+0432 and the wavelength of the merger signal (~10^9 cm; ~10^{-13} eV/c^2), then the considerations concerning the applicability of the GR template given here do not apply. On the other hand, in such a case the combination of binary pulsar and LIGO/VIRGO experiments can be used to constrain the mass of this extra field.

Formation and Past and Future Evolution of the System

The measured spin period, P, and spin-period derivative $\dot{P}$ of PSR J0348+0432, combined with the masses and orbital period of the system (Table 1), form a peculiar set of parameters that gives insight to binary stellar evolution. The short 2.46-hour orbital period is best understood from evolution via a common envelope where the NS is captured in the envelope of the WD progenitor, leading to efficient removal of orbital angular momentum on a short time scale of ~10^3 years (*40*). This implies that the NS was born with an initial mass close to its current mass of 2.01 $M_\odot$, because very little accretion was possible. Whereas the slow spin period of ~39 ms and the unusually strong magnetic field (*8*) of a few 10^9 G (Table 1) provide further support for this scenario, the low WD mass contradicts the standard common-envelope hypothesis by requiring a progenitor star mass smaller than 2.2 $M_\odot$, because more massive stars would leave behind more massive cores (*8*, *41*). For such low donor star masses, however, the mass ratio of the binary components is close to unity, leading to dynamically stable mass transfer without forming a common envelope (*42*, *43*). One potential solution to this mass discrepancy for common-envelope evolution is to assume that the original mass of the WD was ≥0.4 $M_\odot$ and that it was subsequently evaporated by the pulsar wind (*44*) when PSR J0348+0432 was young and energetic, right after its recycling phase (*8*). Such an evolution could also help explain the formation of another puzzling system, PSR J1744−3922 (*45*). However, we find that this scenario is quite unlikely given that the observed spectrum of the WD in PSR J0348+0432 only displays hydrogen lines, which is not expected if the WD was indeed a stripped remnant of a much more massive helium or carbon-oxygen WD. Furthermore, it is unclear why this evaporation process should have come to a complete stop when the WD reached its current mass of 0.17 $M_\odot$. A speculative hypothesis to circumvent the above-mentioned problems would be a common-envelope evolution with hypercritical accretion, where ~0.6 $M_\odot$ of material was efficiently transferred to a 1.4 $M_\odot$ NS (*8*, *46*).

An alternative, and more promising, formation scenario is evolution via a close-orbit low-mass x-ray binary (LMXB) with a 1.0 to 1.6 $M_\odot$ donor star that suffered from loss of orbital angular momentum because of magnetic braking (*43*, *47*, *48*). This requires a finely tuned truncation of the mass-transfer process, which is not yet understood in detail but which is also required for other known recycled pulsars (*8*) with short orbital periods of $P_b \leq 8$ hours and low-mass helium WD companions with $M_{WD} \approx 0.14$ to 0.18 $M_\odot$. The interplay between magnetic braking, angular momentum loss from stellar winds (possibly caused by irradiation), and mass ejected from the vicinity of the NS is poorly understood, and current stellar evolution models have difficulties reproducing these binary pulsar systems. One issue is that the converging LMXBs most often do not detach but keep evolving with continuous mass transfer to more and more compact systems with $P_b \leq 1$ hour and ultralight donor masses smaller than 0.08 $M_\odot$.

By using the Langer stellar evolution code (*8*), we have attempted to model the formation of the PSR J0348+0432 system via LMXB evolution (Fig. 6). To achieve this, we forced the donor star to detach its Roche lobe at $P_b \sim 5$ hours, such that the system subsequently shrinks in size to its present value of $P_b \cong 2.46$ hours because of GW radiation within 2 Gy, the estimated cooling age of the WD. An illustration of the past and future evolution of PSR J0348+0432 from the two different formation channels is shown in Fig. 7.

An abnormality of PSR J0348+0432 in view of the LMXB model is its slow spin period of $P \sim 39$ ms and, in particular, the high value for the spin period derivative, $\dot{P} = 2.41 \times 10^{-19}$ s s^{-1}. These values correspond to an inferred surface magnetic flux density of $B \sim 2 \times 10^9$ G, which is high compared with most other recycled pulsars (*49*). However, a high B value naturally explains the slow spin period of PSR J0348+0432 from a combination of spin-down during the Roche-lobe decoupling phase (*50*) and subsequent magnetic dipole radiation from this high-magnetic-field pulsar (*8*, *49*). Another intriguing question concerning this evolutionary channel is the spread in NS masses. In the five currently known NS-WD systems with $P_b \leq 8$ hours, the NS masses span a large range of values, ranging from ~ 1.4 up to 2.0 $M_\odot$. The lower masses imply that the mass

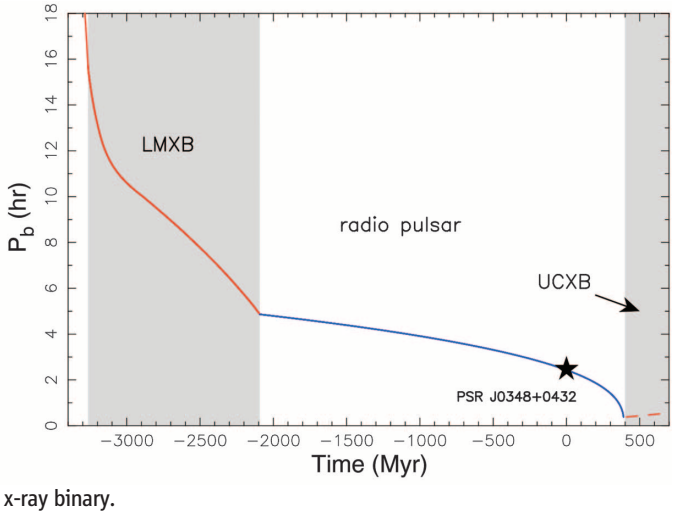

Fig. 6. Past and future orbital evolution of PSR J0348+0432. Formation of PSR J0348+0432 from our converging LMXB model calculation. The plot shows orbital period as a function of time (calibrated to present day). The progenitor detached from its Roche lobe about 2 Gy ago (according to the estimated cooling age of the WD) when $P_b \cong 5$ hours, and since then GW damping reduced the orbital period to its present value of 2.46 hours (marked with a star). UCXB, ultracompact x-ray binary.

transfer during the LMXB phase is extremely inefficient: Only about 30% of the material leaving the donor is accreted by the NS (*14*, *15*). If this is indeed the case and if one assumes that the physical processes that lead to the formation of these systems are similar, it is likely that PSR J0348+0432 was born with an initial mass of $1.7 \pm 0.1\ M_\odot$, providing further support for a non-negligible fraction of NSs born massive (*41*).

Emission of GWs will continue to shrink the orbit of PSR J0348+0432, and in 400 My (when $P_b \cong 23$ min) the WD will fill its Roche lobe and possibly leave behind a planet orbiting the pulsar (*51*, *52*). Alternatively, if PSR J0348+0432 is near the upper-mass limit for NSs, then a BH might form via accretion-induced collapse of the massive NS in a cataclysmic, γ-ray burst–like event (*53*).

Materials and Methods

Radial Velocities and Atmospheric Parameters

A detailed log of the VLT observations can be found in (*8*) (fig. S1 and table S1). We extracted the spectra following closely the method used in (*14*) and compared them with template spectra to measure the radial velocities. Our best fits for the WD had reduced χ^2 minimum values of $\chi^2_{red,\,min} = 1.0$ to 1.5 (*8*). Uncertainties were taken to be the difference in velocity over which χ^2 increases by $\chi^2_{red,\,min}$ to account for the fact that $\chi^2_{red,\,min}$ is not equal to unity (*14*). After transforming the measurements to the reference frame of the solar system barycenter (SSB), we folded them by using the radio-timing ephemeris described below. We then fitted for the semiamplitude of the radial velocity modulation, K_{WD}, and the systemic radial velocity with respect to the SSB, γ, assuming a circular orbit and keeping the time of passage through the ascending node, T_{asc}, fixed to the best-fit value of the radio-timing ephemeris. Our solution yields $K_{WD} = 351 \pm 4$ km s^{-1} and $\gamma = -1 \pm 20$ km s^{-1} (*8*).

Details of the Balmer lines in the average spectrum of PSR J0348+0432, created by the coherent addition of the individual spectra shifted to zero velocity, are shown in Fig. 1B. We modeled the spectrum by using a grid of detailed hydrogen atmospheres (*54*). These models incorporate the improved treatment of pressure broadening of the absorption lines presented in (*55*). As mentioned above, our fit yields $T_{eff} = 10{,}120 \pm 35_{stat} \pm 90_{sys}$ K for the effective temperature and $\log_{10} g = 6.042 \pm 0.032_{stat} \pm 0.060_{sys}$ for the surface gravity (*8*). The χ^2 map shown in Fig. 2A is inflated to take into account systematic uncertainties. The average spectrum was also searched for rotational broadening. By using the analytic profile of (*56*) to convolve the model atmospheres, we scanned the grid of velocities $0 \le v_r \sin i \le 2000$ km s^{-1} with a step size of 100 km s^{-1}. The result is consistent with no rotation and our 1-σ upper limit is $v_r \sin i \le 430$ km s^{-1}.

Modeling of the White Dwarf Mass

Low-mass WDs are thought to form naturally within the age of the universe via mass transfer in a binary, either through Roche-lobe overflow or common-envelope evolution. In both cases, the WD forms when the envelope mass drops below a critical limit, which depends primarily on the mass of the stellar core, forcing the star to contract and detach from its Roche lobe. After the contraction, the mass of the relic envelope is fixed for a given core mass, but further reduction of its size may occur shortly before the star enters the final cooling branch because of hydrogen-shell flashes that force the star to reexpand to giant dimensions. Additional mass removal via Roche-lobe overflow, as well as rapid hydrogen-shell burning through the CNO cycle, may then lead to a decrease of the envelope size and affect the cooling history and atmospheric parameters. To investigate the consequence of a reduced envelope size for the WD companion to PSR J0348+0432, we constructed WD models in which we treat the envelope mass as a free parameter (*8*). For the WD companion to PSR J0348+0432, an envelope mass below the critical limit for hydrogen fusion is not likely for two main reasons.

First, for a pure helium composition, the observed surface gravity translates to a WD mass of ~0.15 $M_\odot$ and a cooling age of ~ 20 My, which is anomalously small. Such a small age would also imply a large increase in the birth and in-spiral rate of similar relativistic NS-WD systems (*57*). Furthermore, postcontraction flash episodes on the WD are not sufficient to remove the entire envelope. Therefore, creation of a pure helium WD requires large mass loss rates before the progenitor contracts, which is unlikely. For small progenitor masses (≤1.5 $M_\odot$), large mass loss prevents contraction, and the star evolves to a semi-degenerate companion on a nuclear time scale that exceeds the age of the universe. For more massive progenitors (>1.5 $M_\odot$), the core grows beyond ~0.17 $M_\odot$ in a short time scale and ultimately leaves a too-massive WD.

Second, even for envelope hydrogen fractions as low as $X_{avg} = 10^{-6}$, the observed temperature and surface gravity cannot be explained simultaneously: The low surface gravity would again require a small mass of ~0.15 $M_\odot$. However, in this case the surface hydrogen acts like an insulator, preventing the heat of the core from reaching the stellar surface. As a result, temperatures as high as 10,000 K can only be reached for masses above ~0.162 $M_\odot$.

Past a critical envelope mass, the pressure at the bottom of the envelope becomes high enough to initiate hydrogen-shell burning. The latter then becomes the dominant energy source, and the

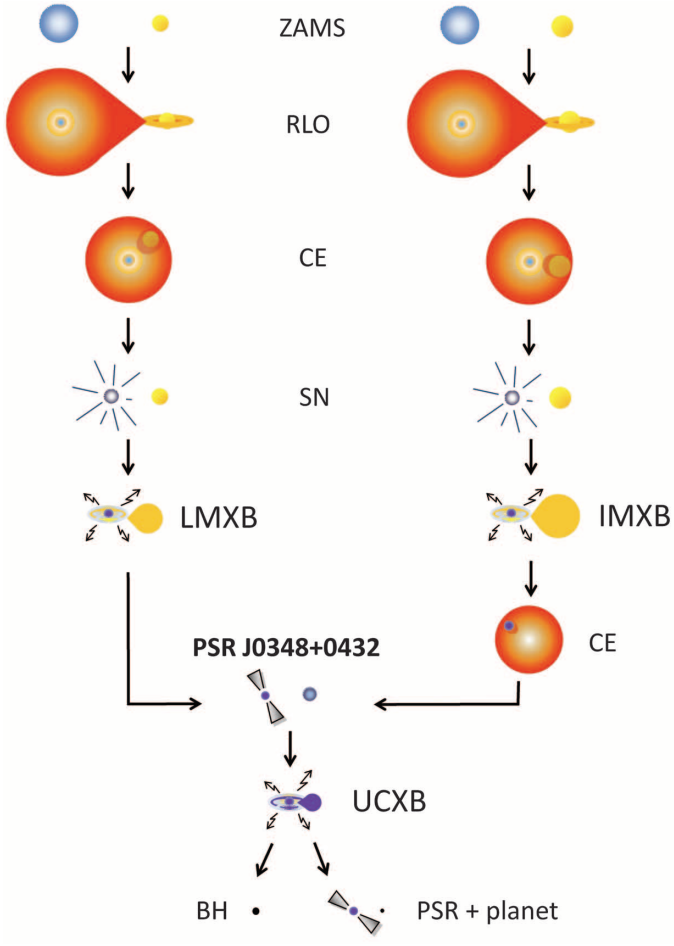

Fig. 7. Possible formation channels and final fate of PSR J0348+0432. An illustration of the formation and evolution of PSR J0348+0432. The zero-age main sequence (ZAMS) mass of the NS progenitor is likely to be 20 to 25 $M_\odot$, whereas the WD progenitor had a mass of 1.0 to 1.6 $M_\odot$ (LMXB) or 2.2 to 5 $M_\odot$ (common envelope, CE), depending on its formation channel. In ~400 My (when $P_b \sim 23$ min), the WD will fill its Roche lobe, and the system becomes an UCXB, leading to the formation of a BH or a pulsar with a planet. RLO, Roche-lobe overflow; SN, supernova; IMXB, intermediate-mass x-ray binary.

evolutionary time scale increases; the radius of the star grows by ~50% (depending on the mass), expanding further for larger envelopes. The dependence of the surface gravity on the radius implies that the observed value translates to a higher mass as the envelope mass increases. Therefore, the most conservative lower limit for the WD mass (and thus for PSR J0348+0432, given the fixed mass ratio) is obtained if one considers models with the absolute minimum envelope mass required for hydrogen burning. In this scenario, the mass of the WD is in the range from 0.162 to 0.181 $M_\odot$ at 99.73% confidence (*8*). Despite this constraint being marginally consistent with our observations (*8*), it is not likely correct because of the high degree of fine-tuning.

For these reasons, we have adopted the assumption that the WD companion to PSR J0348+0432 has a thick envelope, as generally expected for WDs with such low surface gravity and high temperature.

Radio Timing Analysis

The Arecibo observing setup (*8*) and data reduction are similar to the well-tested ones described in (*23*). Special care was taken with saving raw search data, which allows for iterative improvement of the ephemeris and eliminates orbital phase–dependent smearing of the pulse profiles, which might contaminate the measurement of $\dot{P}_b$ (*58*). From this analysis, we derived 7773 independent measurements of pulse times of arrival (TOAs) with a rms uncertainty smaller than 10 μs. Similarly the Effelsberg observations yield a total of 179 TOAs with uncertainties smaller than 20 μs.

We used the tempo2 timing package (*59*) and 8121 available TOAs from GBT (*7*), Arecibo, and Effelsberg to derive the timing solution presented in Table 1. The motion of the radiotelescopes relative to the barycenter of the Solar System was computed by using the DE/LE 421 solar system ephemeris (*60*) published by the Jet Propulsion Laboratory. The orbit of PSR J0348+0432 has a very low eccentricity; therefore, we use the ELL1 orbital model (*61*) to describe the motion of the pulsar.

For the best fit, the reduced χ^2 of the timing residuals (TOA minus model prediction) is 1.66, a result similar to what was obtained in timing observations of other millisecond pulsars. The overall weighted residual rms is 4.6 μs. There are no unmodeled systematic trends in the residuals, either as a function of orbital phase or as a function of time. Therefore $\chi^2 > 1$ is most likely produced by underestimated TOA uncertainties. We increased our estimated TOA uncertainties for each telescope and receiver to produce a reduced χ^2 of unity on short time scales; for our dominant data set (Arecibo), the errors were multiplied by a factor of 1.3.

This produces more conservative estimates of the uncertainties of the timing parameters; these have been verified by using the Monte Carlo statistical method described in (*23*): When all parameters are fitted, the Monte Carlo uncertainty ranges are very similar to those estimated by tempo2. As an example, tempo2 estimates $\dot{P}_b = -2.73 \times 10^{-13} \pm 0.45 \times 10^{-13}$ s s^{-1} (68.27% confidence), and the Monte Carlo method yields $\dot{P}_b = -2.72 \times 10^{-13} \pm 0.45 \times 10^{-13}$ s s^{-1} (68.27% confidence), in excellent agreement. The observed orbital decay appears to be stable; no higher derivatives of the orbital period are detected (*8*).

References and Notes

1. J. M. Lattimer, M. Prakash, The physics of neutron stars. *Science* **304**, 536 (2004). doi: 10.1126/science.1090720
2. P. B. Demorest, T. Pennucci, S. M. Ransom, M. S. Roberts, J. W. Hessels, A two-solar-mass neutron star measured using Shapiro delay. *Nature* **467**, 1081 (2010). doi: 10.1038/nature09466; pmid: 20981094
3. T. Damour, G. Esposito-Farèse, Nonperturbative strong-field effects in tensor-scalar theories of gravitation. *Phys. Rev. Lett.* **70**, 2220 (1993). doi: 10.1103/PhysRevLett.70.2220; pmid: 10053506
4. T. Damour, G. Esposito-Farèse, Tensor-scalar gravity and binary-pulsar experiments. *Phys. Rev. D Part. Fields* **54**, 1474 (1996). doi: 10.1103/PhysRevD.54.1474; pmid: 10020822
5. C. M. Will, *Theory and Experiment in Gravitational Physics* (Cambridge Univ. Press, Cambridge, 1993).
6. J. Boyles *et al.*, The Green Bank Telescope 350 MHz drift-scan survey. I. Survey observations and the discovery of 13 pulsars. *Astrophys. J.* **763**, 80 (2013). doi: 10.1088/0004-637X/763/2/80
7. R. S. Lynch *et al.*, The Green Bank Telescope 350 MHz drift-scan survey. II: Data analysis and the timing of 10 new pulsars, including a relativistic binary. *Astrophys. J.* **763**, 81 (2013). doi: 10.1088/0004-637X/763/2/81
8. Supplementary materials are available on *Science* Online.
9. V. S. Dhillon *et al.*, ULTRACAM: an ultrafast, triple-beam CCD camera for high-speed astrophysics. *Mon. Not. R. Astron. Soc.* **378**, 825 (2007). doi: 10.1111/j.1365-2966.2007.11881.x
10. M. van Kerkwijk, C. G. Bassa, B. A. Jacoby, P. G. Jonker, in *Binary Radio Pulsars*, F. Rasio, I. H. Stairs, Eds. (Astronomical Society of the Pacific Conference Series, San Francisco, CA, 2005) vol. 328, pp. 357–370.
11. A. M. Serenelli, L. G. Althaus, R. D. Rohrmann, O. G. Benvenuto, The ages and colours of cool helium-core white dwarf stars. *Mon. Not. R. Astron. Soc.* **325**, 607 (2001). doi: 10.1046/j.1365-8711.2001.04449.x
12. J. A. Panei, L. G. Althaus, X. Chen, Z. Han, Full evolution of low-mass white dwarfs with helium and oxygen cores. *Mon. Not. R. Astron. Soc.* **382**, 779 (2007). doi: 10.1111/j.1365-2966.2007.12400.x
13. M. Kilic, W. R. Brown, C. Allende Prieto, S. J. Kenyon, J. A. Panei, The discovery of bianry white dwarfs that will merge within 500 Myr. *Astrophys. J.* **716**, 122 (2010). doi: 10.1088/0004-637X/716/1/122
14. J. Antoniadis *et al.*, The relativistic pulsar-white dwarf binary PSR J1738+0333 - I. Mass determination and evolutionary history. *Mon. Not. R. Astron. Soc.* **423**, 3316 (2012). doi: 10.1111/j.1365-2966.2012.21124.x
15. B. A. Jacoby, A. Hotan, M. Bailes, S. Ord, S. R. Kulkarni, The Mass of a Millisecond Pulsar. *Astrophys. J.* **629**, L113 (2005). doi: 10.1086/449311
16. B. Paxton *et al.*, Modules for Experiments in Stellar Astrophysics (MESA). *Astrophys. J.* **192** (suppl.), 3 (2011). doi: 10.1088/0067-0049/192/1/3
17. F. Özel, D. Psaltis, S. Ransom, P. Demorest, M. Alford, The massive pulsar PSR J1614–2230: linking quantum chromodynamics, gamma-ray bursts, and gravitational wave astronomy. *Astrophys. J.* **724**, L199 (2010). doi: 10.1088/2041-8205/724/2/L199
18. A. Dowd, W. Sisk, J. Hagen, *Pulsar Astronomy - 2000 and Beyond, IAU Colloquium 177*, M. Kramer, N. Wex, R. Wielebinski, Eds. (Astronomical Society of the Pacific Conference Series, San Francisco, CA, 2000), vol. 202, pp. 275–276.
19. T. Damour, J. H. Taylor, Strong-field tests of relativistic gravity and binary pulsars. *Phys. Rev. D Part. Fields* **45**, 1840 (1992). doi: 10.1103/PhysRevD.45.1840; pmid: 10014561
20. T. Damour, "Binary systems as test-beds of gravity theories," in *Physics of Relativistic Objects in Compact Binaries: From Birth to Coalescence*, M. Colpi, P. Casella, V. Gorini, U. Moschella, A. Possenti, Eds. (Astrophysics and Space Science Library, Springer, Dordrecht, Netherlands, 2009), vol. 359, pp. 1–41.
21. I. H. Stairs, *Living Rev. Relativ.* **6**, 5 (2003), www.livingreviews.org/lrr-2003-5.
22. M. Kramer *et al.*, Tests of general relativity from timing the double pulsar. *Science* **314**, 97 (2006). doi: 10.1126/science.1132305
23. P. C. C. Freire *et al.*, The relativistic pulsar-white dwarf binary PSR J1738+0333 - II. The most stringent test of scalar-tensor gravity. *Mon. Not. R. Astron. Soc.* **423**, 3328 (2012). doi: 10.1111/j.1365-2966.2012.21253.x
24. C. M. Will, *Living Rev. Relativ.* **9**, 3 (2006), www.livingreviews.org/lrr-2006-3.
25. Y. Fujii, K.-I. Maeda, *The Scalar-Tensor Theory of Gravitation* (Cambridge University Press, Cambridge, 2003).
26. H. Goenner, Some remarks on the genesis of scalar-tensor theories. *Gen. Relativ. Gravit.* **44**, 2077 (2012). doi: 10.1007/s10714-012-1378-8
27. M. Haensel, M. Prószyski, M. Kutschera, *Astron. Astrophys.* **102**, 299 (1981).
28. P. C. C. Freire *et al.*, Eight New Millisecond Pulsars in NGC 6440 and NGC 6441. *Astrophys. J.* **675**, 670 (2008). doi: 10.1086/526338
29. M. H. van Kerkwijk, R. P. Breton, S. R. Kulkarni, Evidence for a massive neutron star from a radial-velocity study of the companion to the black-window pulsar PSR B1957 +20. *Astrophys. J.* **728**, 95 (2011). doi: 10.1088/0004-637X/728/2/95
30. R. W. Romani *et al.*, PSR J1311–3430: A heavyweight neutron star with a flyweight helium companion. *Astrophys. J.* **760**, L36 (2012). doi: 10.1088/2041-8205/760/2/L36
31. J. Alsing, E. Berti, C. M. Will, H. Zaglauer, Gravitational radiation from compact binary systems in the massive Brans-Dicke theory of gravity. *Phys. Rev. D Part. Fields Gravit. Cosmol.* **85**, 064041 (2012). doi: 10.1103/PhysRevD.85.064041
32. www.ligo.org.
33. www.cascina.virgo.infn.it.
34. B. S. Sathyaprakash, B. F. Schutz, *Living Rev. Relativ.* **12**, 2 (2009), www.livingreviews.org/lrr-2009-2.
35. L. Blanchet, *Living Rev. Relativ.* **9**, 4 (2006), www.livingreviews.org/lrr-2006-4.
36. C. M. Will, On the unreasonable effectiveness of the post-Newtonian approximation in gravitational physics. *Proc. Natl. Acad. Sci. U.S.A.* **108**, 5938 (2011). doi: 10.1073/pnas.1103127108; pmid: 21447714
37. M. Maggiore, *Gravitational Waves. Volume 1: Theory and Experiments* (Oxford Univ. Press, Oxford, 2008).
38. C. M. Will, Testing scalar-tensor gravity with gravitational-wave observations of inspiralling compact binaries. *Phys. Rev. D Part. Fields* **50**, 6058 (1994). doi: 10.1103/PhysRevD.50.6058; pmid: 10017576
39. T. Damour, G. Esposito-Farèse, *Phys. Rev. D Part. Fields* **58**, 1 (1998).
40. I. J. Iben, M. Livio, *Publ. Astron. Soc. Pac.* **105**, 1373 (1993).
41. T. M. Tauris, N. Langer, M. Kramer, Formation of millisecond pulsars with CO white dwarf companions - I. PSR J1614–2230: evidence for a neutron star born massive. *Mon. Not. R. Astron. Soc.* **416**, 2130 (2011). doi: 10.1111/j.1365-2966.2011.19189.x
42. T. M. Tauris, G. J. Savonije, *Astron. Astrophys.* **350**, 928 (1999).
43. P. Podsiadlowski, S. Rappaport, E. D. Pfahl, Evolutionary Sequences for Low- and Intermediate-Mass X-Ray Binaries. *Astrophys. J.* **565**, 1107 (2002). doi: 10.1086/324686
44. A. S. Fruchter, J. E. Gunn, T. R. Lauer, A. Dressler, Optical detection and characterization of the eclipsing pulsar's companion. *Nature* **334**, 686 (1988). doi: 10.1038/334686a0

45. R. P. Breton *et al*., The Unusual Binary Pulsar PSR J1744–3922: Radio Flux Variability, Near-Infrared Observation, and Evolution. *Astrophys. J.* **661**, 1073 (2007). doi: 10.1086/515392
46. R. A. Chevalier, Neutron star accretion in a stellar envelope. *Astrophys. J.* **411**, L33 (1993). doi: 10.1086/186905
47. E. Pylyser, G. J. Savonije, *Astron. Astrophys.* **208**, 52 (1989).
48. M. V. van der Sluys, F. Verbunt, O. R. Pols, Reduced magnetic braking and the magnetic capture model for the formation of ultra-compact binaries. *Astron. Astrophys.* **440**, 973 (2005). doi: 10.1051/0004-6361:20052696
49. T. M. Tauris, N. Langer, M. Kramer, Formation of millisecond pulsars with CO white dwarf companions - II. Accretion, spin-up, true ages and comparison to MSPs with He white dwarf companions. *Mon. Not. R. Astron. Soc.* **425**, 1601 (2012). doi: 10.1111/j.1365-2966.2012.21446.x
50. T. M. Tauris, Spin-down of radio millisecond pulsars at genesis. *Science* **335**, 561 (2012). doi: 10.1126/science.1216355
51. M. Bailes *et al*., Transformation of a star into a planet in a millisecond pulsar binary. *Science* **333**, 1717 (2011). doi: 10.1126/science.1208890
52. L. M. van Haaften, G. Nelemans, R. Voss, P. G. Jonker, Formation of the planet around the millisecond pulsar J1719–1438. *Astron. Astrophys.* **541**, A22 (2012). doi: 10.1051/0004-6361/201218798
53. C. D. Dermer, A. Atoyan, Collapse of Neutron Stars to Black Holes in Binary Systems: A Model for Short Gamma-Ray Bursts. *Astrophys. J.* **643**, L13 (2006). doi: 10.1086/504895
54. D. Koester (2008), http://arxiv.org/abs/0812.0482.
55. P.-E. Tremblay, P. Bergeron, Spectroscopic analysis of DA white dwarfs: Stark broadening of hydrogen lines including nonideal effects. *Astrophys. J.* **696**, 1755 (2009). doi: 10.1088/0004-637X/696/2/1755
56. D. F. Gray, *The Observation and Analysis of Stellar Photospheres* (Cambridge Univ. Press, Cambridge, 2005).
57. C. Kim, V. Kalogera, D. R. Lorimer, T. White, The Probability Distribution Of Binary Pulsar Coalescence Rates. II. Neutron Star–White Dwarf Binaries. *Astrophys. J.* **616**, 1109 (2004). doi: 10.1086/424954
58. D. J. Nice, I. H. Stairs, L. E. Kasian, in *40 Years of Pulsars: Millisecond Pulsars, Magnetars and More*, C. Bassa, Z. Wang, A. Cumming, V. M. Kaspi, Eds. (American Institute of Physics Conference Series, Springer, Dordrecht, 2008), vol. 983, pp. 453–458.
59. G. B. Hobbs, R. T. Edwards, R. N. Manchester, tempo2, a new pulsar-timing package - I. An overview. *Mon. Not. R. Astron. Soc.* **369**, 655 (2006). doi: 10.1111/j.1365-2966.2006.10302.x
60. W. M. Folkner, J. G. Williams, D. H. Boggs, *Interplanet. Network Prog. Rep.* **178**, C1 (2009).
61. C. Lange *et al*., Precision timing measurements of PSR J1012+5307. *Mon. Not. R. Astron. Soc.* **326**, 274 (2001). doi: 10.1046/j.1365-8711.2001.04606.x
62. D. Hobbs *et al*., in *Relativity in Fundamental Astronomy: Dynamics, Reference Frames, and Data Analysis, IAU Symposium 261*, S. A. Klioner, P. K. Seidelmann, M. H. Soffel, Eds. (Cambridge Univ. Press, Cambridge, 2010), pp. 315–319.
63. I. Appenzeller *et al*., *Messenger* **94**, 1 (1998).

Acknowledgments: J.A. is a member of the International Max Planck research school for Astronomy and Astrophysics at the Universities of Bonn and Cologne. P.C.C.F. and J.P.W.V. gratefully acknowledge financial support by the European Research Council for the ERC Starting Grant BEACON under contract no. 279702. M.A.M. acknowledges support from a West Virginia Experimental Program to Stimulate Competitive Research Challenge Grant. J.W.T.H. is a Veni Fellow of the Netherlands Foundation for Scientific Research. V.M.K. holds the Lorne Trottier Chair in Astrophysics and Cosmology, a Canada Research Chair, and a Killam Research Fellowship and acknowledges additional support from a Natural Sciences and Engineering Research Council of Canada (NSERC) Discovery Grant, from Fonds Québécois de la Recherche sur la Nature et les Technologies via le Centre de Recherche Astrophysique du Québec and the Canadian Institute for Advanced Research. M.H.v.K. and I.H.S. acknowledge support from NSERC Discovery Grants. V.S.D., T.R.M., and ULTRACAM are supported by the Science and Technology Facilities Council. This work is based on data collected with the VLT of the European Southern Observatory (ESO) under program 088.D-0138A and observations with the 100-m Effelsberg telescope of the Max Planck Institute for Radioastronomy. The Arecibo Observatory is operated by SRI International under a cooperative agreement with the NSF (AST-1100968) and in alliance with Ana G. Méndez-Universidad Metropolitana and the Universities Space Research Association. The National Radio Astronomy Observatory is a facility of the NSF operated under cooperative agreement by Associated Universities, Incorporated. We are grateful to D. Koester and J. Panei *et al*. for providing models presented in their publications. We are obliged to J. Smoker (ESO) for his help during the VLT observations and D. Champion for assistance with the Effelsberg observations and useful discussions. We also thank D. Lorimer, J. Bell-Burnell, G. Esposito-Farèse, E. Keane, P. Podsiadlowski, and B. Schutz for helpful discussions. This research made use of NASA's Astrophysics Data System and M. T. Flanagan's Java Scientific Library (www.ee.ucl.ac.uk/~mflanaga).

Supplementary Materials

www.sciencemag.org/content/340/6131/1233232/suppl/DC1
Supplementary Text
Figs. S1 to S11
Tables S1 to S3
References (*63*–*112*)

27 November 2012; accepted 6 March 2013
10.1126/science.1233232